

# Increasing Efficiency of Two-Photon Excited Fluorescence and Second Harmonic Generation Using Ultrashort Pulses

Shuo Tang, Tatiana B. Krasieva, Zhongping Chen, Gabriel Tempea\*, and Bruce J. Tromberg  
Laser Microbeam and Medical Program, Beckman Laser Institute,  
University of California, Irvine, CA 92612  
\*Femtolasers Produktions GmbH, A-1100 Vienna, Austria

## ABSTRACT

Multiphoton microscopy (MPM) has become an important tool for high-resolution and non-invasive imaging in biological tissues. However, the efficiencies of two-photon excited fluorescence (TPEF) and second harmonic generation (SHG) are relatively low because of their nonlinear nature. Therefore, it is critical to optimize laser parameters for most efficient excitation of MPM. Reducing the pulse duration can increase the peak intensity of excitation and thus potentially increase the excitation efficiency. In this paper, a multiphoton microscopy system using a 12 fs Ti:Sapphire laser is reported. With adjustable dispersion pre-compensation, the pulse duration at the sample location can be varied from 400 fs to sub-20 fs. The efficiencies of TPEF and SHG are studied for the various pulse durations, respectively. Both TPEF and SHG are found to increase proportionally to the inverse of the pulse duration for the entire tested range. To transmit most of the SHG and TPEF signals, the spectral transmission window of the detection optics needs to be carefully considered. Limitation from phase-matching in SHG generation is not significant because the effective interaction length for SHG is less than 10  $\mu\text{m}$  at the focal depth of the objectives. These results are important in improving MPM excitation efficiency using ultrashort pulses. MPM images from human artery wall are also demonstrated.

**Keywords:** Multiphoton microscopy, two-photon excited fluorescence, second harmonic generation, ultrashort pulse.

## 1. INTRODUCTION

Multiphoton microscopy (MPM), combining two-photon excited fluorescence (TPEF) and second harmonic generation (SHG), has become an important tool for high-resolution, non-invasive imaging of thick biological tissues [1]-[6]. In TPEF, fluorescence from endogenous and exogenous fluorophores is excited by two-photon absorption. TPEF has been widely used for studies of cellular morphology and physiology [1, 2, 3]. SHG is a nonlinear scattering process where two excitation photons are converted into light that is half the wavelength of the excitation light. Strong SHG signals have been observed from fibrillar collagen, the most abundant extracellular matrix (ECM) protein in tissues [4, 5, 6]. Therefore, SHG imaging provides an important technique for studies of physiological processes that involve ECM remodeling such as cancer and wound healing. TPEF and SHG imaging have been combined together to provide complementary co-registered information about cellular and extracellular matrix structures [7, 8]. However, the efficiencies of TPEF and SHG excitation are very low in biological tissues because they are both nonlinear processes. Tissues are also highly scattering, a phenomenon that causes light intensity to drop off rapidly with excitation depth. Therefore, it is of great interest to increase MPM excitation efficiency in tissues by optimizing the spatial, spectral, and temporal properties of laser sources [9, 10, 11].

Generally, femtosecond pulsed lasers are required in order to increase the peak intensity of excitation. Increasing the average laser intensity can improve the signal levels of TPEF and SHG. However, this can result in greater tissue damage and loss of cell viability. An alternate approach involves increasing peak laser power by reducing pulse duration while maintaining average intensity. McConnell and Riis observed a sevenfold increase in TPEF yield when laser pulses were compressed from 250 fs to 35 fs [12]. Xu and Webb examined the impact of pulse durations from 60 fs to 1.2 ps on TPEF for pulses measured before the objective and they observed an inverse relationship between TPEF signal and pulse duration [13]. In Müller et al. [14], optical pulses of 15 fs duration were achieved at the focal plane of high N.A. objectives and a significant increase in TPEF was observed. Recent advances in laser technology have made pulsed lasers of sub-20 fs duration commercially available and thus multiphoton microscopy

systems using sub-20 fs pulses have become practical. Dispersion-compensated sub-20 fs laser pulses allow for excitation of TPEF and SHG signals with greater efficiency. In practical terms, this can result in enhanced tissue imaging depths and higher frame rates.

In this paper, we report the development of a multiphoton microscopy system using a 12 fs Ti:Sapphire laser. The techniques of characterizing ultrashort pulses and compensating dispersion are discussed in Sections 2 and 3, respectively. With a prism-pair dispersion compensator, we have achieved sub-20 fs pulses at the focal plane of high N.A. objectives. In Section 4, we study how the TPEF and SHG efficiencies can be influenced by pulse duration. It is observed that the TPEF and SHG intensities increase inversely as pulse duration is shortened from 400 fs to sub-20 fs. With sub-20 fs pulses, we can excite MPM signals highly efficiently. Using ultrashort pulses it is possible to relax the requirement on tight focusing in spatial domain and to develop wide-field MPM in the future. In Section 5, we show MPM images from the study of vulnerable plaque in human artery. The images are obtained with a relative low N.A. 10× objective and cover a large area of 500 μm × 500 μm. Section 6 concludes the paper.

## 2. CHARACTERIZATION OF ULTRASHORT PULSES

Ultrashort optical pulses can be characterized by an autocorrelator. There are two configurations of the autocorrelators which measure the interferometric and intensity autocorrelation, respectively. Figure 1 shows the two configurations in (a) interferometric autocorrelation and (b) intensity autocorrelation. In both cases the laser beam is split into two beams which go through different delay lines. In Fig. 1(a), the two beams are recombined together to be overlapping and collinear. The combined beam then shines on a nonlinear crystal to generate second order nonlinear signal (often second harmonic signal). The fundamental signal is removed by a filter and the second harmonic signal is detected by a detector. When the time delay between the two beams is scanned, an interferometric autocorrelation trace is obtained. A typical interferometric autocorrelation trace is shown in Fig. 1(a). The full width at half maximum (FWHM) of the trace envelope indicates the width of the short pulse. The interference fringes are internal calibration of time because each fringe corresponds to the traveling time of light over a distance of a wavelength. Therefore, interferometric autocorrelation is accurate in characterizing ultrashort optical pulses in the sub-20 fs regime because of the internal calibration.

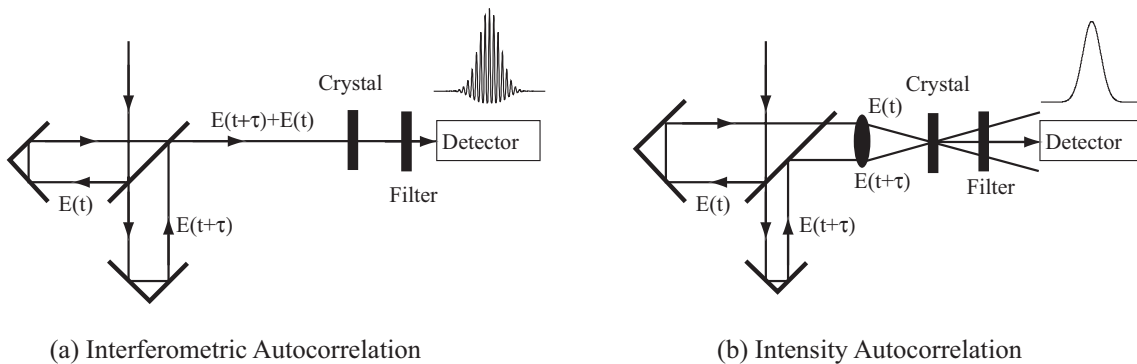


Figure 1: Principle of autocorrelation.

In Fig. 1(b), after the delay lines the two beams are collinear but shifted in space. After a focusing lens, the two laser beams cross each other at the focus. The nonlinear crystal is placed at the focal plane where the two beams cross each other. After removing the fundamental beam by the filter, we can observe three SHG signal spots. The central one is generated by the interaction between the two beams while the two side spots are generated by each individual laser beam independently. For intensity autocorrelation we are only interested in the center SHG signal spot which can be selected by a pinhole in front of the detector. A typical intensity autocorrelation trace is also shown in the figure and there is only the envelope trace of the pulse without interference fringes. Therefore, the intensity autocorrelation trace needs to be calibrated for absolute pulse durations. Meanwhile, the intensity autocorrelation is not sensitive to phase variations in the pulses so that it is a better measurement of the intensity profile when chirping is present in the pulses.

The mathematical form of autocorrelation can be described as follows. The detector measures the intensity of SHG signal which is proportional to the square of the amplitude of the SHG electric field. Meanwhile, SHG is a second

order nonlinear process in which the electric field of SHG is proportional to the square of the input laser field. In the autocorrelation measurement, the input laser field is the addition of two laser fields delayed in time. We can write the electric field as  $E(t) = |E(t)| \cdot e^{-i\omega t + i\varphi(t)}$  where  $|E(t)|$  is the amplitude of the electric field,  $\omega$  is the angular frequency of the light, and  $\varphi(t)$  is the slowly varying phase term related to chirping. The delayed field can be written similarly. Overall, the autocorrelation signal should be  $I(\tau) = \int_{-\infty}^{+\infty} |E(t) + E(t + \tau)|^4 dt$ . Expanding this expression we

can get four terms as follows:

$$I(\tau) = \int_{-\infty}^{+\infty} |E(t)|^4 dt + \int_{-\infty}^{+\infty} |E(t + \tau)|^4 dt \quad (1)$$

$$+ \int_{-\infty}^{+\infty} 4 \cdot |E(t)|^2 \cdot |E(t + \tau)|^2 dt \quad (2)$$

$$+ \int_{-\infty}^{+\infty} 4 \cdot \left[ |E(t)|^2 + |E(t + \tau)|^2 \right] \cdot |E(t)| \cdot |E(t + \tau)| \cdot \cos(\omega \cdot \tau - \Delta\varphi(t)) dt \quad (3)$$

$$+ \int_{-\infty}^{+\infty} 2 \cdot |E(t)|^2 \cdot |E(t + \tau)|^2 \cdot \cos(2 \cdot \omega \cdot \tau - 2 \cdot \Delta\varphi(t)) dt \quad (4)$$

In the above four terms, the 1<sup>st</sup> term is a constant background SHG signal which is generated by individual beams; the 2<sup>nd</sup> term is the intensity autocorrelation term which indicates the intensity pulse width and shape; the 3<sup>rd</sup> and 4<sup>th</sup> terms contribute to the interference fringes under the envelop of the interferometric autocorrelation. In the interferometric autocorrelation, the signal includes all the four terms as shown above. The interferometric autocorrelation is sensitive to chirping because the variable  $\Delta\varphi(t) = \varphi(t + \tau) - \varphi(t)$  is related to phase variations of the laser beam coming from the 3<sup>rd</sup> and 4<sup>th</sup> terms. Meanwhile, the intensity autocorrelation only has the 2<sup>nd</sup> term of the above expression.

### 3. DISPERSION PRECOMPENSATION

When using ultrashort pulses for multiphoton microscopy, pulse broadening due to temporal dispersion is a critical issue. Without appropriate dispersion precompensation, femtosecond pulses can be easily stretched to picosecond pulses by dispersion from the beam delivery optics. The major dispersive component in MPM is the high N.A. objective. The total amount of dispersion from the beam delivery path including the objective can be precompensated by a prism pair arranged in a setup such as shown in Fig. 2. The input laser beam hits the apex of the first prism (left) and the light is spread in space due to spatial dispersion of the prism. The spread laser beam passes through the 2<sup>nd</sup> prism (right) and all the wavelength components become collinear but shifted in space. A mirror folds the beam backward so that light passes through the whole setup twice, doubling the beam path and recombining the wavelength components in space. The input and output laser beams can be separated by a beam splitter or by slightly tilting the angle of the mirror. The prisms used are usually Brewster prisms to minimize the loss. The material can be fused silica to minimize third order dispersion or SF10 to increase the amount of dispersion compensated.

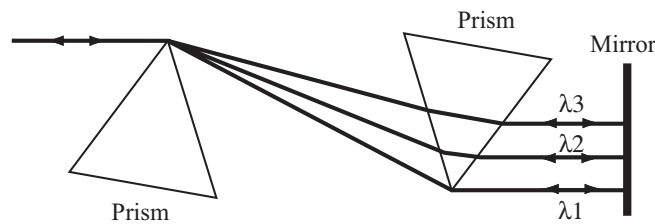


Figure 2: Prism pair for dispersion precompensation.

In ordinary optics, the longer wavelength light (red light) usually travels faster than the shorter wavelength light (blue light). This is called positive dispersion. This is why ultrashort pulses which have a broad bandwidth will have the spectral components stretched out in time due to the different traveling speed. A prism-pair compensates such stretching by introducing spatial dispersion which causes different wavelengths to travel over different optical path lengths in space. As in the prism-pair design for dispersion compensation, the red light is forced to travel over a longer distance than the blue light so that we can slow down the red light. This is called negative dispersion. The amount of negative dispersion is controlled by the separation between the apexes of the two prisms as well as the insertion of the 2<sup>nd</sup> prism (on the right) into or out of the beam path in the normal direction to the bottom of the prism.

#### 4. TPEF AND SHG EFFICIENCY VS. PULSE DURATION

We have designed a MPM system using a 12 fs Ti:Sapphire laser (Femtolasers) as the excitation source. With the 12 fs laser source we hope to increase the MPM excitation efficiency because of the high peak power provided by the ultrashort pulses. The schematics of the MPM system is shown in Fig. 3. The center wavelength of the laser is 800 nm with a bandwidth of ~100 nm. The laser output first passes through a pair of fused silica Brewster prisms for dispersion precompensation which has been discussed in Section 3. In this setup, the amount of dispersion precompensated is controlled by the separation between the two prisms. The laser beam after the prism pair is angled slightly to be separated from the input beam. Afterwards, the laser beam is sent to two galvanometer mirrors for raster scanning. The scanned laser beam is expanded by two lenses before entering the back entrance of the objective. A tightly focused laser beam is delivered to the sample by the objective. The emitted TPEF and SHG signals from the sample are collected by the same objective lens in a backward direction. The emitted signals are separated from the excitation by a dichroic mirror (675DCSP, Chroma). A short-pass filter can be used to further remove residue excitation laser light. TPEF and SHG are separated by a second dichroic mirror (475DCLP, Chroma) and selected by suitable band-pass filters. In the imaging mode, the separated TPEF and SHG signals are detected by two photomultiplier tubes, respectively. In the spectral mode, the emitted signals are collected by a fiber bundle after the 675DCSP dichroic mirror and sent to a spectrograph (SpectraPro-150, Acton Research) with a grating of 300 grooves blazed at 500 nm, followed by a cooled CCD camera (NTE/CCD-512-EBFT, Princeton Instrument).

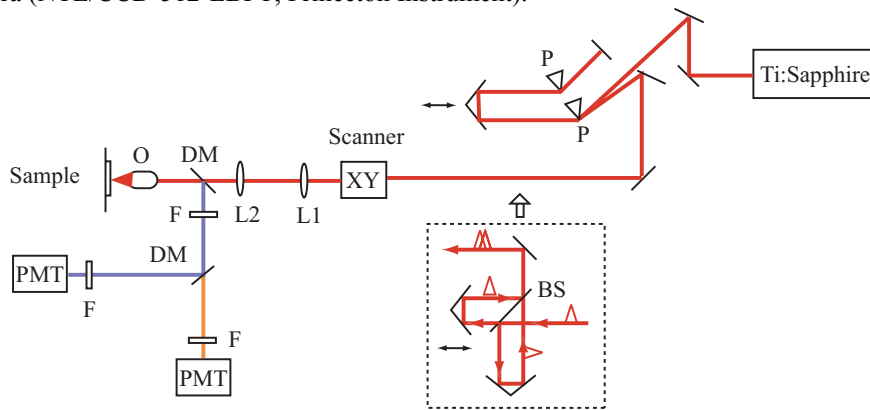


Figure 3: Schematics of the MPM system.

To obtain highest excitation efficiency of MPM, we need to minimize the pulse duration at the sample location. Measuring ultrashort pulses at the tight focus of the objective is very challenging. Since the laser beam is tightly focused by the objective, the working distance is not enough to insert a standard autocorrelator (as shown in Fig. 1) for pulse characterization. An alternate way is to separate the delay lines and the detector in the autocorrelation measurement [15]. As shown in Fig. 3, the unit of splitting the laser beam and introducing time delay is inserted into the MPM setup before the XY scanner. The laser beam after this unit is collimated and overlapped in space but has two sequences of pulses delayed in time. The nonlinear material for autocorrelation measurement is placed at the focal plane of the objective. This nonlinear material can be an SHG crystal (for example BBO) or a two-photon fluorescence dye solution (for example fluorescein). The excited 2<sup>nd</sup> order nonlinear signal is detected by the PMTs in the MPM setup. In

this way, we can measure interferometric autocorrelation right at the focal plane. However, in the presence of chirping, the FWHM of the interferometric autocorrelation is largely influenced and thus is not an accurate representation of the pulse width. In such a case, intensity autocorrelation is a better way to measure the pulse duration. Therefore, for intensity autocorrelation measurements we relocated lens 1 of the beam expander as shown in Fig. 3 to a position after the objective so that the laser beam would not be tightly focused. Thus, intensity autocorrelation is measured with the autocorrelator in a standard setup as in Fig. 1(b). We found a close match between pulse durations measured with the interferometric and intensity autocorrelations when the dispersion was well compensated. However, for severely dispersed pulses which do not have standard pulse shape and phase information, it is more reliable to measure the intensity autocorrelation than the interferometric autocorrelation.

In the experiment, our laser output has pulses of 12 fs duration. After the beam delivery path and the dispersion precompensation in the MPM system, we have characterized sub-20 fs pulses at the focal plane. Thus we expect to increase the MPM excitation efficiency using our sub-20 fs pulses compared with traditional MPM systems using >100 fs pulses. In the next, we study the excitation efficiencies of SHG and TPEF using pulses of different durations. The pulse duration is adjusted by varying the apex separation between the prisms. The shortest laser pulses delivered to the sample location are achieved when the dispersion from the objective and all the other optics in the beam pass is well compensated. Longer pulses are delivered when the dispersion is under compensated, where a large amount of chirping is introduced. Therefore, we can study how the TPEF and SHG signals change with different pulse durations. For this study, a dilute fluorescein solution was used to generate TPEF signals, and a freshly excised rat-tail tendon was used to generate SHG. Two objective lenses, a Plan-Neofluoar 10× of 0.3 N.A. and a water immersion Achroplan 40× of 0.8 N.A. from Zeiss, were studied, respectively.

From the theory, TPEF and SHG signals depend quadratically on the instantaneous excitation intensity. For pulsed excitation, the measured two-photon signals are averaged over time so that their averaged values should depend on  $\langle I(t)^2 \rangle$ , where  $I(t)$  is the instantaneous laser intensity and  $\langle \cdot \rangle$  denotes the operation of time average. Because the measurement of pulsed laser power is also averaged over time, the two-photon signals should be proportional to  $\langle I(t)^2 \rangle = g_p \langle I(t) \rangle^2 / (R \tau_p)$ , where  $\langle I(t) \rangle$  is the averaged laser intensity,  $\tau_p$  is the pulse duration,  $R$  is the pulse repetition rate, and  $g_p$  is a constant which depends on pulse shape [3]. Therefore, theoretically the two-photon signals should be proportional to  $\tau_p^{-1}$  if the average laser intensity is constant.

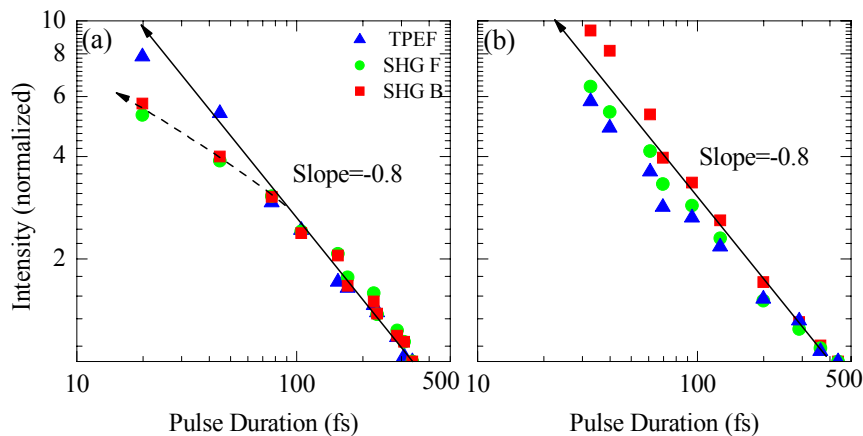


Figure 4: MPM signal intensity vs. pulse duration. (a) With a short-pass filter. (b) Without the short-pass filter.

Figure 4 shows the intensities of the TPEF and SHG signals excited from samples with laser pulses of different durations from 400 fs to sub-20 fs measured with intensity autocorrelations. When the pulse duration was varied, the average laser power was maintained at a constant level. The intensities of TPEF and SHG are normalized to one, respectively, at the excitation with the longest pulse measured in the experiment. The SHG intensities from the rat-tail tendon were actually measured in both forward and backward propagation directions for the interest of studying the directionality of SHG generation. At the begin, our results showed some difference between the behaviors of the TPEF and SHG signals. As shown in Fig. 4(a), the TPEF increases consistently when the pulse duration is shortened. However, the increase of SHG signal seems to slow down when the pulse gets shorter than 100 fs. First we thought this might be affected by phase matching condition in SHG generation. However, later on we found that the reduction of

SHG efficiency at shorter pulses were actually due to spectrum cut off by the short-pass filter which we used to remove residue fundamental laser beam. After we removed this filter, it is found that the SHG signal increased consistently as well as the TPEF signal when the pulse duration was shortened to the sub-20 fs regime. This is shown in Fig. 4(b). In Fig. 4(b), our experimental results show a dependence of TPEF and SHG proportional to  $\tau_p^{-0.8}$  which agrees well with the theoretical predication. The deviation is due to changes in pulse shape that are unavoidable when long pulses are generated by under dispersion compensation. Figure 4 shows the TPEF and SHG signals obtained with the 40 $\times$  objective. With the 10 $\times$  objective, we have got similar results with continues increase in MPM efficiency when the pulses are shortened. These results demonstrate that significant improvement in excitation efficiency can be achieved by shortening the laser pulses. Such improvement continues as the pulse duration is shortened to the sub-20 fs regime. This result holds true for both high and low N.A. objectives.

The filtering effect is proved by measuring the spectrum of MPM signal and the transmission window of the filter. In the design of an MPM system, the spectral response of the system is very critical because from the fundamental excitation beam to the SHG beam the total spectrum covers from 800 nm to 400 nm. In the excitation beam path, we need to transmit as much as possible the light around 800 nm excitation wavelength. In the detection beam path, we need to collect most of the TPEF and SHG signals while filtering the fundamental 800 nm beam. Different from confocal fluorescence microscopy, the emission in MPM is at a shorter wavelength than the excitation. Therefore, short-pass filters are usually used to separate the emission from the excitation. However, short-pass filters do not pass all the short wavelengths due to the material transmission limitation. If not specially designed, the short-pass filters often cut off the wavelength shorter than 400 nm. As shown in Fig. 5, the filter is a short-pass E650SP from Chroma. As we can see the transmission window is from 400 nm to 650 nm. Shorter than 400 nm the light would not transmit either. This imposes a problem on MPM microscopy because in MPM we also want to detect SHG which is right around the edge of 400 nm. This problem is especially critical when using ultrashort pulses which has a broad bandwidth. A broad fundamental bandwidth will excite SHG at a broad bandwidth too. Fig. 5 also shows the spectrum of the excited SHG and TPEF signals from human skin. The spectrum has two distinctive peaks. The sharp peak around 400 nm is SHG signal from collagen and the much broader peak around 500 nm is due to TPEF from the cells. The spectrum peak of SHG is sharp when compared with the TPEF signal. Nevertheless, our SHG signal peak is still much broader than SHG spectrum excited with a narrow band laser such as the Mira laser. The SHG spectrum is at about the edge of the transmission window of many optical materials. When designing MPM system, it is very critical to select the right optical material for the optimal efficiency of excitation and collection.

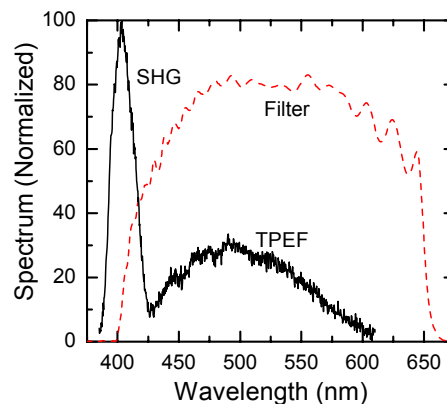


Figure 5: Spectrum of SHG and TPEF signals in comparison with the filter transmission bandwidth.

Although TPEF and SHG signals are both quadratically dependent on instantaneous laser power, their mechanisms are quite different. TPEF signals are incoherent and isotropic while SHG signals are coherent and directional. Although poor phase-matching can reduce SHG efficiency, there is no significant difference in the efficiencies of TPEF and SHG up to sub-20 fs pulse excitation. In addition, while the absolute values of the SHG intensities in forward and backward directions are quite different, the  $\tau_p^{-1}$  dependence is identical in both propagation directions. These phenomena may be due to the fact that the effective length for SHG generation is only a few microns within the focal depths of the objectives. The effect of phase matching is not critical when the SHG effective length is shorter than 10  $\mu\text{m}$  for pulses longer than 20 fs.

## 5. MPM IMAGES OF HUMAN ARTERY

The significant increase in TPEF and SHG signal intensities using ultrashort laser pulses has important implications for nonlinear microscopy. As the excitation efficiency is improved, we can potentially image deeper into thick tissues and increase frame rates. In MPM microscopy, the excitation laser beam is usually tightly focused in spatial domain to increase the photon flux. Now as we can use ultrashort pulses to obtain extremely high peak laser intensity, it can relax the requirement on the spatial focusing. Therefore, by manipulating the laser beam in time domain, we can possibly achieve wide field illumination in MPM which will reduce imaging time when acquiring information from a large area.

Since our excitation laser pulses are extremely short, we can excite MPM signals very efficiently. Even with a 10× objective, we can get very strong TPEF and SHG signals. Figure 6 shows the TPEF and SHG signals from a human artery imaged with the 10× objective. In human artery there is a disease called vulnerable plaque. When fatty components start to build up in the artery, they create a lipid pool in the artery wall as shown in the cartoon of Fig. 6(b). When the lipid pool expands and the capsule between the artery lumen and the lipid pool thins, the plaque becomes vulnerable to rupture which can cause serious health problem. In our study, we have imaged a fatty streak area which has the deposition of lipids and also a lesion area where the plaque has already ruptured. In comparison we also imaged the normal healthy artery wall as control. Figure 6(c) shows a photo of the sample and the different regions that we have imaged. The imaging areas shown in Fig. 6(a) are 500 μm × 500 μm. As we compare the normal, fatty, and lesion areas, we see distinctive structural differences among the three regions. In the normal area, we see a well organized network of connective tissue structure. The SHG signal is presumably generated by the collagen fibers. The TPEF signal can be generated by elastin fibers and cells. It is also possible to excite TPEF signal from collagen since our laser has a very broad bandwidth. In the fatty area, we see big holes of exclusion of both SHG and TPEF signals. Those holes are possibly the lipid deposition within the connective tissue in the artery wall. In the lesion area, the tissue becomes highly scattering with little structure.

The MPM signals imaged with the 10× objective is still currently obtained by scanning the laser beam. Nevertheless, we demonstrate that, with a relatively low N.A objective., we can still efficiently excite MPM signals. To eventually develop wide field MPM, the illumination spot of the laser beam will further be increased to eventually eliminate the need of beam scanning.

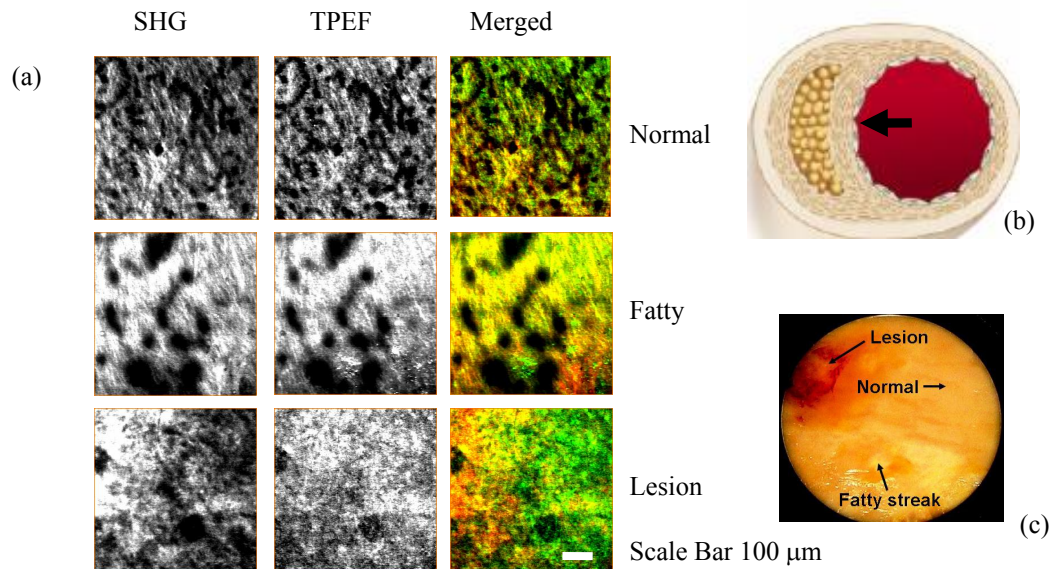


Figure 6: (a) SHG and TPEF images of human artery wall. (b) Cartoon of artery plaque. (c) Photo of sample.

## 6. CONCLUSIONS

In conclusion, we have studied the effect of pulse duration on the generation of TPEF and SHG signals in nonlinear optical microscopy. The ultrashort pulses are generated by a 12 fs Ti:Sapphire laser. The pulses are characterized with both interferometric and intensity autocorrelations. Sub-20 fs pulses are obtained at the focal plane after the dispersion is precompensated by a prism-pair. When tuning the pulse durations, both the TPEF and SHG efficiencies are found to increase proportionally to the inverse of pulse duration even in the sub-20 fs regime. There is no significant reduction of SHG efficiency due to the phase-matching condition because the effective SHG interaction length is very short at the focus of the objectives. However, the spectral filtering effect from limited bandwidth response of the collection optics needs to be carefully considered when detecting SHG signal near the 400 nm wavelength. MPM images from the study on vulnerable plaque in human artery demonstrate the efficient MPM excitation using the sub-20 fs pulses in our system. The potential indicates the possibility of developing wide-field MPM using temporal focusing with pulses < 20 fs in the future.

## ACKNOWLEDGMENT

This work was supported by the National Institute of Health Laser Microbeam and Medical Program (RR01192), Air Force Office of Scientific Research, Beckman Foundation, and Whitaker Foundation.

## REFERENCES

1. W. Denk, J.H. Strickler, and W.W. Webb, "Two-photon laser scanning fluorescence microscopy," *Science*, vol. 248, pp. 73-76, Apr. 1990.
2. K. König, "Multiphoton microscopy in life sciences," *J. Microsc.*, vol. 200, pp. 83-104, Nov. 2000.
3. W.R. Zipfel, R.M. Williams, and W.W. Webb, "Nonlinear magic: multiphoton microscopy in the biosciences," *Nature Biotechnol.*, vol. 21, pp. 1369-1377, Nov. 2003.
4. P.J. Campagnola, M.D. Wei, A. Lewis, and L.M. Loew, "High-resolution nonlinear optical imaging of live cells by second harmonic generation," *Biophys. J.*, vol. 77, pp. 3341-3349, Dec. 1999.
5. P.J. Campagnola, H.A. Clark, W.A. Mohler, A. Lewis, and L.M. Loew, "Second-harmonic imaging microscopy of living cells," *J. Biomed. Opt.*, vol. 6, pp. 277-286, Jul. 2001.
6. P. Stoller, B.M. Kim, A.M. Rubenchik, K.M. Reiser, and L.B.D. Silva, "Polarization-dependent optical second-harmonic imaging of a rat-tail tendon," *J. Biomed. Opt.*, vol. 7, pp. 205-214, Apr. 2002.
7. A. Zoumi, A. Yeh, and B.J. Tromberg, "Imaging cells and extracellular matrix in vivo by using second-harmonic generation and two-photon excited fluorescence," *Proc. Natl. Acad. Sci. USA*, vol. 99, pp. 11014-11019, Aug. 2002.
8. A.T. Yeh, B.S. Kao, W.G. Jung, Z.P. Chen, J.S. Nelson, and B.J. Tromberg, "Imaging wound healing using optical coherence tomography and multiphoton microscopy in an in vitro skin-equivalent tissue model," *J. Biomed. Opt.*, vol. 9, pp. 248-253, Mar./Apr. 2004.
9. R. Wolleschensky, T. Feuerer, R. Sauerbrey, and U. Simon, "Characterization and optimization of a laser-scanning microscope in the femtosecond regime," *Appl. Phys. B*, vol. 67, pp. 87-94, 1998.
10. J. Squier and M. Müller, "High resolution nonlinear microscopy: a review of sources and methods for achieving optimal imaging," *Rev. Sci. Instrum.*, vol. 72, pp. 2855-2867, Jul. 2001.
11. P.N. Marsh, D. Burns and J.M. Girkin, "Practical implementation of adaptive optics in multiphoton microscopy," *Opt. Express*, vol. 11, pp. 1123-1130, May 2003.
12. G. McConnell and E. Riis, "Two-photon laser scanning fluorescence microscopy using photonic crystal fiber," *J. Biomed. Opt.*, vol. 9, pp. 922-927, Sep./Oct. 2004.
13. C. Xu, W.W. Webb, "Measurement of two-photon excitation cross sections of molecular fluorophores with data from 690 to 1050 nm," *J. Opt. Soc. Am. B*, vol. 13, pp. 481-491, Mar. 1996.
14. M. Müller, J. Squier, R. Wolleschensky, U. Simon, and G.J. Brakenhoff, "Dispersion pre-compensation of 15 femtosecond optical pulses for high-numerical-aperture objectives," *J. Microsc.*, vol. 191, pp. 141-150, Aug. 1998.
15. M. Müller, J. Squier, and G.J. Brakenhoff, "Measurement of femtosecond pulses in the focal point of a high-numerical-aperture lens by two-photon absorption," *Opt. Lett.*, vol. 20, pp. 1038-1040, May 1995.